



HAL
open science

Trends of Coastal Sea Level Between 1993 and 2015: Imprints of Atmospheric Forcing and Oceanic Chaos

Thierry Penduff, W. Llovel, Sally Close, Ixetl Garcia-Gomez, Stéphanie
Leroux

► **To cite this version:**

Thierry Penduff, W. Llovel, Sally Close, Ixetl Garcia-Gomez, Stéphanie Leroux. Trends of Coastal Sea Level Between 1993 and 2015: Imprints of Atmospheric Forcing and Oceanic Chaos. *Surveys in Geophysics*, 2019, 10.1007/s10712-019-09571-7 . hal-02323701

HAL Id: hal-02323701

<https://hal.science/hal-02323701>

Submitted on 23 Apr 2020

HAL is a multi-disciplinary open access archive for the deposit and dissemination of scientific research documents, whether they are published or not. The documents may come from teaching and research institutions in France or abroad, or from public or private research centers.

L'archive ouverte pluridisciplinaire **HAL**, est destinée au dépôt et à la diffusion de documents scientifiques de niveau recherche, publiés ou non, émanant des établissements d'enseignement et de recherche français ou étrangers, des laboratoires publics ou privés.



Distributed under a Creative Commons Attribution 4.0 International License

Trends of Coastal Sea Level Between 1993 and 2015: Imprints of Atmospheric Forcing and Oceanic Chaos

Thierry Penduff¹  · William Llovel²  · Sally Close¹  · Ixetl Garcia-Gomez¹  · Stéphanie Leroux³ 

Abstract

The observation and simulation of the variability of coastal sea level are impacted by various uncertainties, such as measurement errors and sampling biases, unresolved processes, and model and forcing biases. Ocean model simulations suggest that another uncertainty should be taken into account for the attribution of sea-level changes. Global ocean simulations indeed show that resolving mesoscale turbulence (even partly) promotes the emergence of low-frequency (LF) chaotic intrinsic variability (CIV) which causes substantial random fluctuations of sea level up to multiple decades in eddy-active regions of the world ocean. This random LFCIV is superimposed on the atmospherically forced (or simply “forced”) fluctuations, which are directly controlled by the atmospheric variability. We show from a large ensemble of global oceanic hindcasts that this multi-decadal LFCIV leaves a substantial imprint on the long-term trends (1993–2015) of coastal sea level: over 17–20% of the global ocean coastal area, in particular along the coastlines of the northwestern Pacific and Indian Oceans, and around the Gulf of Mexico, random sea-level trends may blur their atmospherically forced counterpart, such that simulated (and potentially observed) coastal sea-level trends cannot be unambiguously attributed to atmospheric or anthropic causes. The steric and manometric sea-level change contributions of these uncertainties are discussed, suggesting that they mostly come from the manometric sea-level trends near the coasts.

Keywords Sea-level trend · Coastal ocean · Ensemble modeling · Intrinsic variability · Detection and attribution

✉ Thierry Penduff
Thierry.Penduff@cnr.fr

¹ CNRS, IRD, Grenoble-INP, Institut des Géosciences de l’Environnement (IGE-MEOM), Université Grenoble Alpes, CS 40 700, Grenoble, France

² Laboratoire d’Études en Géophysique et Océanographie Spatiales (LEGOS)/CNRS/IRD/CNES/UPS, OMP, 14 Avenue Edouard Belin, 31400 Toulouse, France

³ Ocean Next, 90 Chemin du Moulin, 38660 La Terrasse, Grenoble, France

1 Introduction and Context

1.1 Open Ocean and Coastal Sea-Level Evolution

The remote observation of sea level has reached an unprecedented level of accuracy and spatio-temporal coverage with the launch of the Topex/Poseidon altimeter satellite in 1992, followed by several successors up to the present day. Data from these successive missions have been inter-calibrated and merged into gridded fields, providing a continuous quasi-global monitoring of sea level at a spatio-temporal resolution ranging from the scale of mesoscale eddies to the global ocean, and from weekly timescales to more than two decades (Ablain et al. 2017; WCRP Global Sea Level Budget Group 2018). These data have yielded tremendous progress in physical oceanography for the description, understanding, modeling, and forecasting of the evolution of sea level (as well as related variables, including below the surface) over a wide range of scales.

Anthropogenic global warming is mostly being transferred to the ocean (Church et al. 2011; Rhein et al. 2013) and has a particularly clear imprint on global mean sea level, with a linear rise of $3 \pm 0.4 \text{ mm year}^{-1}$ since 1993 (Nerem et al. 2018). This globally averaged increase is mostly due to the thermal expansion of sea water (known as thermosteric sea-level contribution), and to the melting of ice sheets from Greenland and Antarctica and mountain glaciers. The continental freshwater input has a global imprint on global mean sea-level rise and is known as barystatic sea-level rise (Gregory et al. 2019). At regional scale, other physical processes are at play such as salinity changes that can compensate or enhance temperature changes (Llovel and Lee 2015), ocean dynamics and circulation (affecting seawater properties), atmospheric heat fluxes, precipitation, and evaporation (Church et al. 2013). The observed trends of sea level in fact have a complex and slowly varying spatial structure controlled by many oceanic and atmospheric processes, the geometry of ocean basins and coasts, the vertical displacements of the latter, etc. This means that in certain coastal regions, the observed sea-level trend can be substantially smaller or larger than its global average, raising in the latter case serious environmental concerns within highly populated coastal areas around the globe.

The monitoring, understanding, and mitigation of sea-level changes require accurate and stable measurements of open ocean and coastal sea level over long periods (see Marcos et al. 2019), together with numerical and process-oriented studies of the ocean dynamics. Another important issue also requires attention: it concerns the estimation of uncertainties associated with the measurements and processes of long-term sea-level variations, which are particularly large in coastal regions.

1.2 Low-Frequency Chaotic Intrinsic Variability (LFCIV) in the Ocean

One specific uncertainty about the low-frequency oceanic variations of regional sea level has been somewhat overlooked until recently and is now being recognized as substantial in the open ocean. Global ocean/sea-ice simulations, and especially those performed in the eddying regime (with grid spacings of $1/4^\circ$ and finer) show that nonlinear ocean dynamics spontaneously produce a *Low-Frequency Chaotic Intrinsic Variability (LFCIV)*, even without any low-frequency atmospheric forcing. Penduff et al. (2011) and Sérazin et al. (2015) have shown from long global ocean/sea-ice high-resolution simulations, repeatedly forced by the same annual cycle, that the LFCIV leaves a large imprint on sea level in many

regions of the open ocean, and may explain in certain midlatitudes eddy-active regions up to 100% of the *full* interannual-to-decadal sea-level variability simulated in a *hindcast*.¹ This LFCIV questions the attribution to atmospheric or anthropic drivers of regional sea-level variability or long-term changes: the LFCIV in the turbulent ocean consists of a persistent low-frequency spatially-structured “noise” (with a random phase and an intermittent character) that may blur or even dominate the “signal” (i.e., the atmospherically *forced* variations) that is directly driven by the evolution of the external forcing. It is important to note that LFCIV is much weaker in non-turbulent ocean models² (Penduff et al. 2011), suggesting that the coarse-resolution ocean components of coupled climate models used for climate projections largely underestimate this source of uncertainty.

Sérazin et al. (2018) demonstrated that nonlinear interactions between mesoscale (turbulent, chaotic) eddies at subannual timescales spontaneously and persistently feed sea-level variability at longer timescales (i.e., decadal in the Southern Ocean).³ This temporal inverse cascade is at work in $1/4^\circ$ and $1/12^\circ$ global ocean simulations; this process is basically equally strong under seasonal atmospheric forcing and under full reanalyzed forcing, and may thus be an important source of LFCIV in oceanic hindcasts.

1.3 Disentangling the LFCIV and the Atmospherically Forced Ocean Variability

The model studies mentioned above took advantage of pairs of simulations: a climatological run that isolates the LFCIV under repeated seasonal forcing, and a hindcast (driven by an atmospheric reanalysis including interannual variability) that simulates the “full” low-frequency ocean variability. These results suggested that the full ocean variability in this eddying regime might be a blend of LFCIV and atmospherically forced variability (Penduff et al. 2011). Pairs of simulations, however, are not sufficient to properly disentangle both components.

In order to separate both components, the OCCIPUT project produced a large ensemble (50 members) of $1/4^\circ$ -resolution global ocean/sea-ice NEMO-based simulations (Penduff et al. 2014, Bessières et al. 2017). As explained in the next section, the integration strategy was designed to separate, quantify, and characterize the *forced* variability that is directly driven by the atmospheric variability, and the chaotic intrinsic variability (abbreviated as LFCIV for low frequencies) whose phase differs in each member, and which is independent of the atmospheric evolution.

Studies based on $1/4^\circ$ and $1/12^\circ$ climatological simulations have shown that the LFCIV not only has a strong imprint on sea level, but also on the Atlantic Meridional Overturning simulation (AMOC; see Hirschi et al. 2003; Grégorio et al. 2015). Analyses of the OCCIPUT ensemble have further demonstrated that the LFCIV, now diagnosed from ensemble statistics, remains comparable in amplitude to its counterpart in climatological runs (Leroux et al. 2018), and impacts other important climate-relevant oceanic variables: the interannual-to-decadal variability of ocean heat content (OHC) was, for example, shown to be dominantly chaotic in several regions of the global ocean (Sérazin et al. 2017).

¹ That is, a simulation driven by an atmospheric reanalysis, i.e., including the full range of timescales.

² Certain 1° -resolution simulations produce LFCIV, albeit with much weaker intensity (e.g., O’Kane et al. 2013).

³ Although other processes such as large-scale baroclinic instability may also produce LFCIV (Huck et al. 2015).

While the globally integrated OHC interannual-to-decadal variability is almost totally forced by the atmosphere in the OCCIPUT ensemble, the LFCIV impact on certain large-scale climate-relevant oceanic indices can remain substantial at very large spatial scales. Zanna et al. (2018) thus showed that between 40 and 48°S, the LFCIV accounts for about 30% of the monthly to multi-decadal variability of the Meridional Heat Transport integrated over the whole range of longitudes.

1.4 Impacts of the Forcing and of the LFCIV on Long-Term Oceanic Trends

The chaotic component of the eddying ocean variability can exert a significant influence even at timescales of multiple decades and thus has an imprint on long-term trends. Sérazin et al. (2016) showed from a long climatological 1/4° NEMO simulation that multi-decadal LFCIV in strongly eddying regions may manifest itself as *random sea-level trends* over several decades. Sérazin et al. (2017) further showed that in such regions the 30-year trends of OHC fields, computed between 1980 and 2010 from the OCCIPUT ensemble, may also be mostly due to the oceanic chaos and not to the atmospheric (or anthropogenic) forcing. Llovel et al. (2018) showed that similar results hold for regional sea-level trends in many regions of the open ocean over the altimetric period (1993–2015).

These results strongly suggest that attributing low-frequency ocean variability, and certain long-term trends, to external (atmospheric, or anthropogenic) drivers is not straightforward in the eddying ocean. The ocean-driven multi-decadal LFCIV may manifest itself in certain finite-length time series as significant random trends. This raises important issues regarding the detection and attribution of oceanic changes in numerical simulations, and presumably in observations.

The aforementioned studies were, however, focused on the impacts of the LFCIV and atmospheric variability in the open ocean and gave no particular consideration to coastal regions. In this study, the OCCIPUT ensemble simulation is analyzed to disentangle the respective imprints of the atmospheric forcing and the low-frequency oceanic chaos on regional sea-level trends over the altimetric period (1993–2015), in particular in coastal regions. This paper addresses the following questions:

- How are the forced and random sea-level trends distributed in the coastal ocean?
- Where is the signal-to-noise ratio (ratio between the forced and random trends) largest and smallest in the coastal ocean?
- What are the contributions of steric and manometric (i.e., non-steric or bottom pressure changes, Gregory et al. 2019) effects in the forced and random sea-level trends in the coastal ocean?
- What are the implications of the above issues for the monitoring, analysis and forecast of sea-level trends?

Section 2 presents the OCCIPUT ensemble simulation, and the post-processing applied to the model outputs. Section 3 presents the respective imprints of forced and random sea-level trends, with a specific focus on coastal and shallow regions. Conclusions are given and discussed in the last section.

2 Post-processing of Model and Observed Data

The partners of the OCCIPUT project (Oceanic Chaos—ImPacts, strUcture, predicTability, Penduff et al. 2014) performed two kinds of $1/4^\circ$ ocean/sea-ice simulations drawing on a common global model configuration based on NEMO3.5 (Bessières et al. 2017): the ensemble run presented above consists in 50 hindcasts with perturbed initial conditions, driven over 1960–2015 by the DFS5.2 forcing fields (based on ERA-Interim, see Dussin and Barnier 2013); a companion climatological simulation was repeatedly forced during 330 years by a climatological atmospheric annual cycle derived from DFS5.2. (This forcing is devoid of any low-frequency and trend.) The integration strategy is detailed in Leroux et al. (2018) and is summarized below.

2.1 Ensemble Simulation Strategy

All members of the ensemble simulation were initialized using the final state of a common 21-year spin-up. We then introduced slight stochastic perturbations within each ensemble member during 1960 (see Brankart 2013 and Bessières et al. 2017), switched off these perturbations at the end of 1960, and resumed the integration of the 50 members until 2015 using the same fully varying DFS5.2 forcing. Nonlinear ocean dynamics yield an initial growth of incipient perturbations, i.e., of chaotic mesoscale anomalies; the subsequent ensemble spread then approximately saturates in amplitude within a few months or years depending on the region (see Zanna et al. 2018). Nonlinear processes (e.g., eddy–eddy interactions, subsequent spatial and temporal inverse cascades) then contribute to extend the range of chaotic fluctuations toward lower wavenumbers and frequencies, hence feeding the LFCIV and larger structures which emerge around the ensemble mean within each member with a random phase. As shown in Sérazin et al. (2016) under seasonal forcing, and in Sérazin et al. (2017) and in Llovel et al. (2018) in the OCCIPUT ensemble, the LFCIV exerts an influence on decadal and longer periods as the OCCIPUT simulation proceeds, and leaves regional imprints on long-term trends in the form of random trends within each member. The present paper will assess whether (coastal) sea-level trends are also impacted by this random signal.

2.2 Computing Regional Sea-Level Trends

The full details of the post-processing are presented in Llovel et al. (2018) and summarized below. The diagnostics performed in this study started in 1993, i.e., after $21 + 34 = 55$ years of dynamical adjustment within each member. At every grid point of each ensemble member, we first compute the linear trend of sea level over the 23-year period 1993–2015. The imprint of the model numerical drift on sea-level trends is then estimated from the climatological run in a similar way: the drift-related linear sea-level trend is computed at every grid point from the climatological run after 55 years of adjustment, i.e., between years 56 and 78. This field is removed from the trends of the 50 ensemble members to retain the geophysical sea-level trend signals. Finally, we subtract the global average from these 50 sea-level trend fields (this being necessary in Boussinesq ocean models, see Greatbatch 1994), yielding 50 estimates of regional sea-level trends over 1993–2015, corrected for the model drift and relative to their global average. These processing steps yield a remarkably small root-mean-square difference between observed and ensemble mean sea-level trends (1.57 mm/year over the period 1993–2015, see Llovel et al. 2018).

Consistently with the above, steric sea-level fields are calculated from the monthly 3-dimensional temperature and salinity fields archived from the 50 ensemble members (between 1993 and 2015) at every grid point. We estimate the spurious drift of 3-D temperature and salinity from the climatological run (between years 56 and 78), remove this drift from the 3-D temperature and salinity fields from the 50 members, compute the full-depth steric sea-level trend fields, and finally remove their respective global averages. This yields 50 regional steric sea-level trend fields, corrected for the model drift and relative to their global average. Manometric sea-level trends are computed from each ensemble member as the difference between sea-level trends and full-depth steric sea-level trends. Note that manometric sea-level trends refer to the ocean bottom pressure term in regional sea-level changes (see Gregory et al. 2019 for more details).

The observed regional sea-level trend field is calculated over the same 1993–2015 period from the Climate Change Initiative (CCI, Legeais et al. 2018) dataset derived from several altimeter missions. The observed regional sea-level trend field is finally obtained by removing the global average from the latter field and used to assess the realism of the ensemble simulation.

2.3 Ensemble Statistics: Forced and Random Trends

The ensemble standard deviation (ESTD) of any oceanic field simulated with this initial perturbation ensemble modeling strategy quantifies the imprint of the chaotic variability on this field (i.e., the width of the ensemble spread). The ensemble mean (EMEAN) of any field provides an estimate of the atmospherically forced signal, since all members were driven by the same atmospheric forcing. For the purpose of this study, we estimated the forced sea-level trend (due to external influences, i.e., atmospheric variability and trend, anthropogenic influences, etc.) by the ensemble mean of the 50 sea-level trend maps, and the imprint of low-frequency chaotic variability by the ensemble standard deviation of these maps (which will quantify the amplitude of random trends in the following). These forced and random signals are estimated for the total, steric, and manometric regional sea-level trends. Using the Lilliefors test, we verified that local ensemble distributions of total and steric sea-level trend fields are Gaussian at the 95% significance level over 93% of the global ocean area. The use of EMEANs and ESTDs to estimate the forced and random trends is therefore adequate for our analysis.

3 Results from the 1/4° OCCIPUT Ensemble Simulation

Section 3.1 describes and compares the forced and random sea-level trends in the open ocean and summarizes the more detailed analysis presented by Llovel et al. (2018). The focus is put on coastal regions in the following sections.

3.1 Forced and Random Regional Sea-Level Trends in the Open Ocean

Figure 1a, b shows the regional trends of sea level over the period 1993–2015 from altimeter observations and from a randomly picked OCCIPUT member (member #1), respectively. While some discrepancies are visible in certain regions (in particular in the North Atlantic western Subpolar Gyre), the distribution and magnitude of regional sea-level trends are quite well reproduced by the model: Llovel et al. (2018) show that the

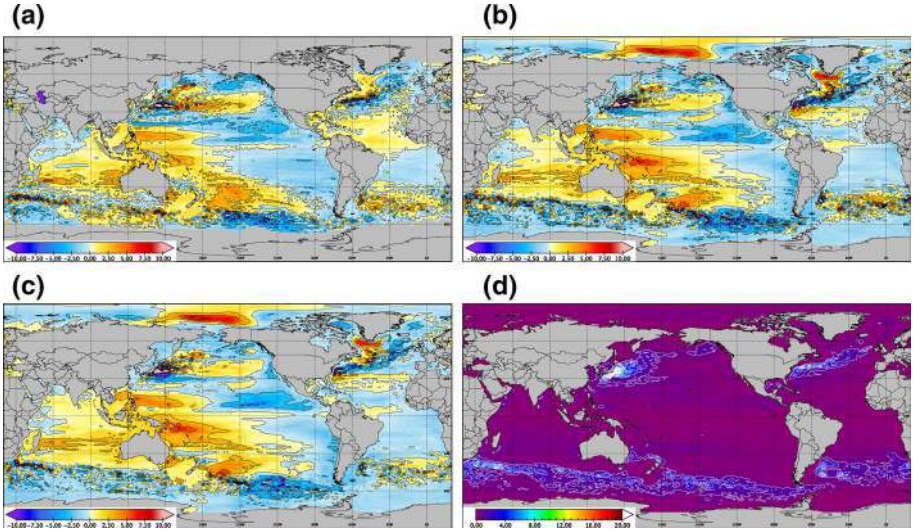


Fig. 1 1993–2015 regional sea-level trends from the CCI observational product (a) and from the OCCIPUT ensemble simulation: ensemble member #1 (b), forced trends (c, ensemble mean), and random trends (d, ensemble standard deviation)

root-mean-square difference between OCCIPUT and observed trends is smaller than any simulation considered in Griffies et al. (2014). Large-scale patterns of regional sea-level trends range between roughly -3 and $+3$ mm/year, and are found at similar locations in the model and the real ocean: large positive trends throughout most of the western Pacific and within the subtropical gyres of the South Indian, South Atlantic, and North Atlantic oceans; large negative trends over most of the eastern and southern Pacific, and along the Gulf Stream path.

We now take advantage of the information from the 50 members and split the simulated sea-level trends into their forced (EMEAN, Fig. 1c) and random (ESTD, Fig. 1d) components. The main large-scale patterns of regional sea-level trends simulated in member #1 happen to belong to the forced component over many regions (compare panels b and c); there indeed, random trends (panel d) remain smaller than about 1 mm/year, i.e., smaller than forced trends. The relative contributions of forced and random trends should, however, be compared more quantitatively to identify regions where the “signal,” associated with the atmospheric fluctuations and climate change, can be considered as significantly larger than the “noise,” associated with LFCIV.

We define at every grid point a signal-to-noise ratio (SNR) as the ratio of the absolute value of the forced sea-level trend to the random sea-level trend, respectively, given by the EMEAN and ESTD of local trends. The larger the SNR, the more confidently one can attribute the regional sea-level trend found in one particular realization (i.e., one ensemble member picked randomly) to the external forcing, whether it be natural atmospheric variability or anthropogenic influences. Conversely, the smaller the SNR the more the low-frequency chaotic variability impacts the sea-level trends in a given realization, with a smaller impact of external sources. As Sérazin et al. (2017, their section 4), we consider that one may attribute the regional trend found in a given realization to the external forcing where $\text{SNR} > 2$, while one cannot unambiguously do so

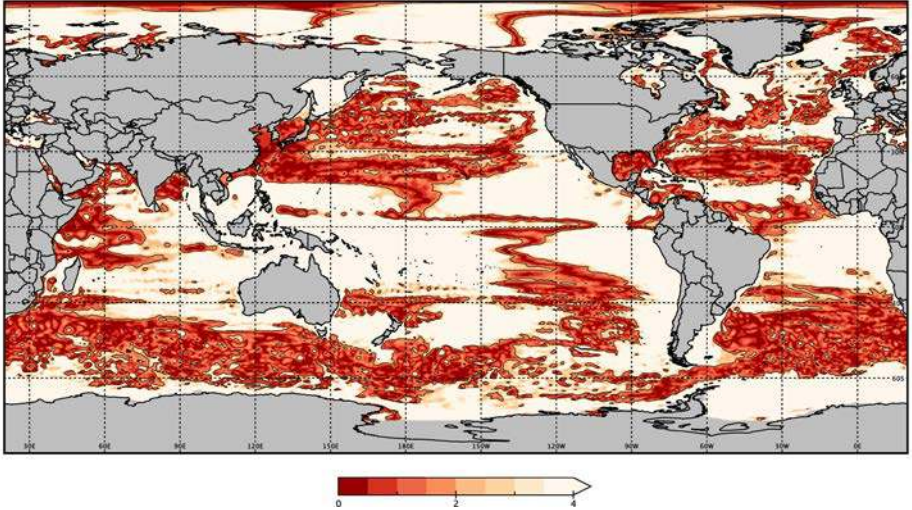


Fig. 2 Ratio between the forced and random 1993–2015 regional sea-level trends (i.e., ensemble mean divided by the ensemble standard deviation, or signal-to-noise ratio) deduced from the OCCIPUT ensemble simulation. Sea-level trends found in a single member cannot be unambiguously attributed to the atmospheric forcing (95% confidence interval) in regions enclosed by the $\text{SNR}=2$ isocontour (black)

where $\text{SNR} < 2$ (at the 95% confidence level). In other words, regional sea-level trends in regions where $\text{SNR} < 2$ may just be random since they emerge from the LFCIV.

Figure 2 shows the global distribution of the sea-level trend SNR, and the black contour encircles regions where $\text{SNR} < 2$. Large forced trends are generally associated with large SNRs in vast areas of the intertropical Pacific, within most of the Eastern Pacific and Arctic oceans. This is no longer the case in many other parts of the global ocean: $\text{SNR} < 2$ over most of the South Atlantic ($25\text{--}55^\circ\text{S}$), central and tropical parts of the North Atlantic ($15\text{--}45^\circ\text{N}$, $0\text{--}10^\circ\text{N}$), western North Pacific ($18\text{--}50^\circ\text{N}$, west of 180°W), western Indian ocean (west of 60°E , from 15°S to the northern boundary), and almost everywhere in the Antarctic Circumpolar Current (except in the South Pacific sector). There, our results suggest that regional sea-level trends are not certainly driven by external (atmospheric or anthropogenic) causes, but may be random since they are influenced by the intrinsic oceanic “noise” (LFCIV). In other words, sea-level trends in such regions are affected by a sizeable uncertainty due to chaotic ocean dynamics.

3.2 Forced and Random Regional Sea-Level Trends in Coastal Regions

Figure 2 shows that the SNR increases and passes the $\text{SNR}=2$ threshold when approaching the coast in several regions, such as around Alaska, Antarctica, Australia and all islands located north of it, around all islands from Cuba to the lesser Antilles, or along the west coasts of America, Europe, and North Africa. Figure 3d shows that the coasts surrounding the southern tip of Africa (SA region) seem to be shielded from the very small SNR values found offshore within the strongly chaotic Agulhas Retroflexion. Along other coastlines, however, the opposite holds: the other panels of Fig. 3 show that over large coastal parts of the northwestern Pacific (NWP), western Indian

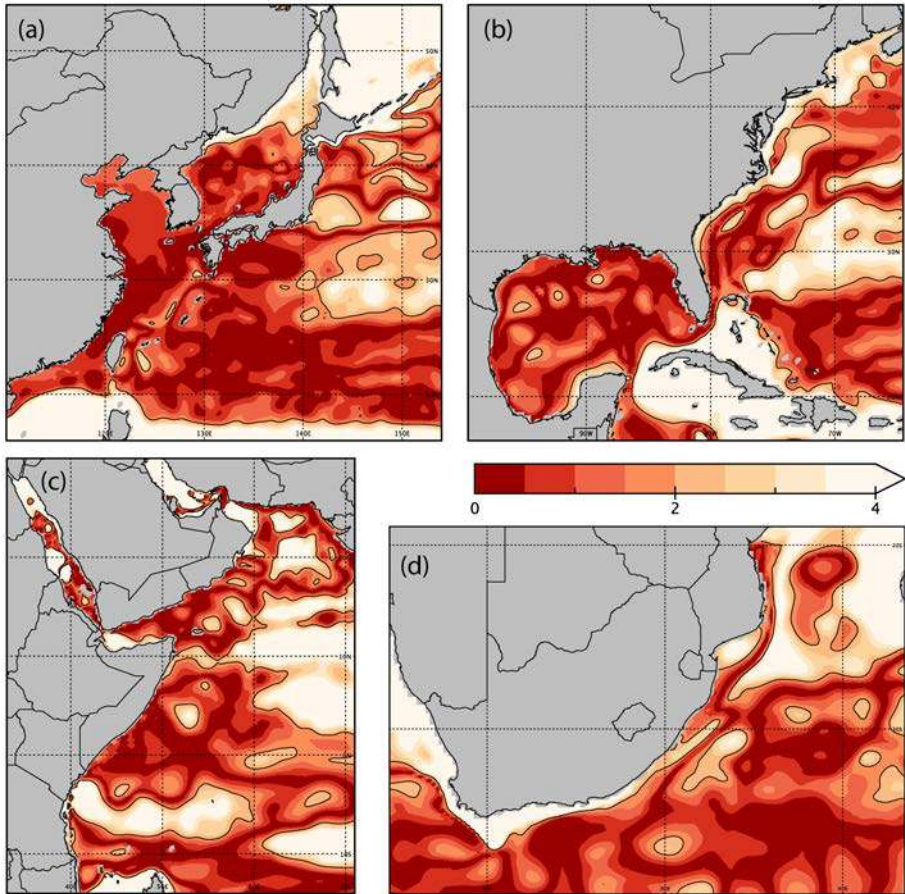


Fig. 3 Zooms of Fig. 2 in the Northwest Pacific (a), the Northwest Atlantic (b), the Northwest Indian (c), and around the south of Africa

(WI), Gulf of Mexico, and US east coast (MEX), the SNR remains smaller than 2 and may even fall below 0.5 locally. In the latter coastal regions, the modeled sea-level trends may thus be random and cannot be unambiguously attributed to the atmospheric (and anthropogenic) forcing.

We now try to identify generic differences between the open ocean and coastal regions in terms of forced and random sea-level trends (and/or their ratio, SNR). We will focus on five specific domains: the global ocean, and the four domains shown in Fig. 3. We will show the distributions of forced trends, random trends, and SNR considering all grid points of each specific domain, then considering two subregions within each specific domain: the coastal domain (CD) will include all grid points located less than 25 km away from the coastline, whether they be deep or shallow. In a complementary way, the shallow domain (SD) will include all grid points where depth is shallower than 25 m, whether they be close to or far away from the coasts.

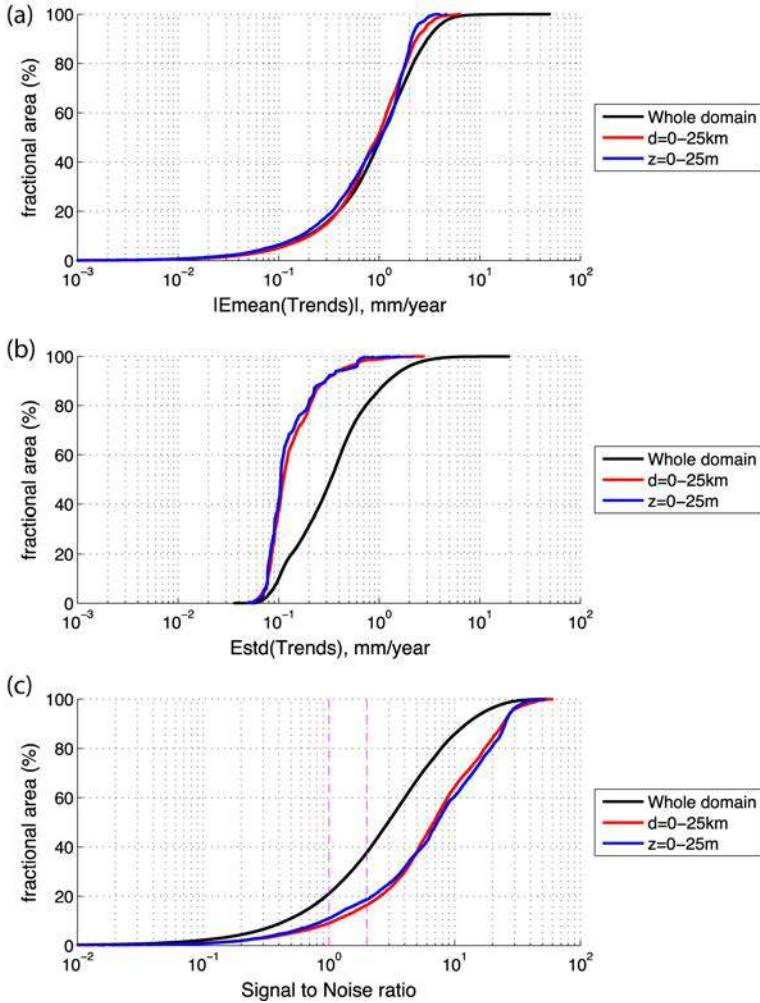


Fig. 4 Cumulative fractional area of the global ocean as a function of: **a** absolute value of the forced sea-level trends; **b** random sea-level trends; **c** local signal-to-noise ratio shown in Fig. 2. Black lines show the results for all model points, red lines for model points located within 0–25 km from the coasts, blue lines for model points located in regions shallower than 25 m

3.2.1 Scale of the global ocean

Let us first consider the global ocean domain. We sort in increasing order the signals (i.e., the absolute value of the forced sea-level trends) simulated at each grid point of the domain; we accumulate the areas of the corresponding grid points and express the result as a fraction (in %) of the total area of the domain. This result is shown in black in Fig. 4a (the fractional area is not shown for very small values of the signal): this line indicates for instance that the absolute value of forced sea-level trends is smaller than 0.4 mm/year over 20% of the global ocean area, smaller than 1 mm/year (the median) over half of it, larger than 3 mm/year over 10% of it, and does not exceed 50 mm/year anywhere. The same

computation is done in the CD and SD subregions of the global ocean, and the results are shown in red and blue in the same figure. The differences between these 3 lines are generally small (median values are around 1 mm/year in the 3 regions), except for the largest signals: the signal exceeds 3 mm/year within only 5% of the area of CD, and barely anywhere in SD. We thus conclude that at global scale, the distribution of forced sea-level trends in shallow and coastal regions is comparable to their counterparts in the open ocean, except for extreme (and rare) signals which are much smaller near the coast.

The same three computations are repeated in the global ocean, substituting the signal with the noise (i.e., random trends or ensemble standard deviation). Figure 4b shows that noise values range between about 0.035 and 20 mm/year at global scale, with a median of 0.3–0.4 mm/year, that is 30–40% of the median of the signal. Unlike the signal however, the noise substantially decreases (by a factor of about 3 for the median, 10 for the maximum) when focusing on shallow (SD) and coastal (CD) domains. This reduction might be explained by one or several of the following hypotheses: the mesoscale processes that emerge and may locally feed LFCIV may be marginally resolved by the model since internal deformation radii are smaller in shallow regions (see, e.g., Hallberg 2013); the time-scales of the LFCIV generated in these regions may not reach multiple decades and have less imprint on long-term trends; the multi-decadal LFCIV present in the neighboring open ocean may be high-pass filtered when approaching the coasts and shallow waters. Other hypotheses might exist, and further work is required to explain these features, which nevertheless are quite robust according to Fig. 4b.

Figure 4c does not show the ratio of the lines in the previous two panels, but presents the result of the binning described above applied to local SNR values within the global ocean, and its CD and SD subdomains. The black line shows that sea-level trends can be considered to be dominantly driven by the atmosphere over more than half (62%) of the global open ocean area (where $\text{SNR} > 2$). Colored lines show that regional sea-level trends in coastal and shallow parts of the global ocean are characterized by larger SNR values than in the open ocean: the SNR remains larger than 2 in about 80–83% of their area; the coastal areas are also those where the largest values of the SNR may be found at global scale.

These model results conversely show that within 17–20% of the coastal and shallow areas of the global ocean, the 1993–2015 sea-level trends are likely to be random because of LFCIV and are not certainly forced by external drivers. This proportion decreases from 38 to 17–20% from the open ocean to the shallow and coastal domains because the imprint of LFCIV on sea-level trends significantly decreases there. In other words, the model suggests that the attribution of observed sea-level trends (from altimetry or from tide gauges) to non-oceanic sources is questionable over 38% of the global ocean area, and over about one-fifth of the coastal and shallow water area. The implications of these results are further discussed in the last section of this paper.

3.2.2 Zoom on Four Specific Regions

We now describe in more detail the respective imprints of the external forcing and of the oceanic chaos on sea-level trends in the four regional domains shown in Fig. 3, and in their coastal (CD) and shallow (SD) parts.

We saw that coastal SNR values tend to remain small in the region surrounding the Southern tip of Africa (SA, Fig. 3d). Figure 5d shows that the SNR changes from the whole SA domain to its shallow and coastal parts are comparable to those described at

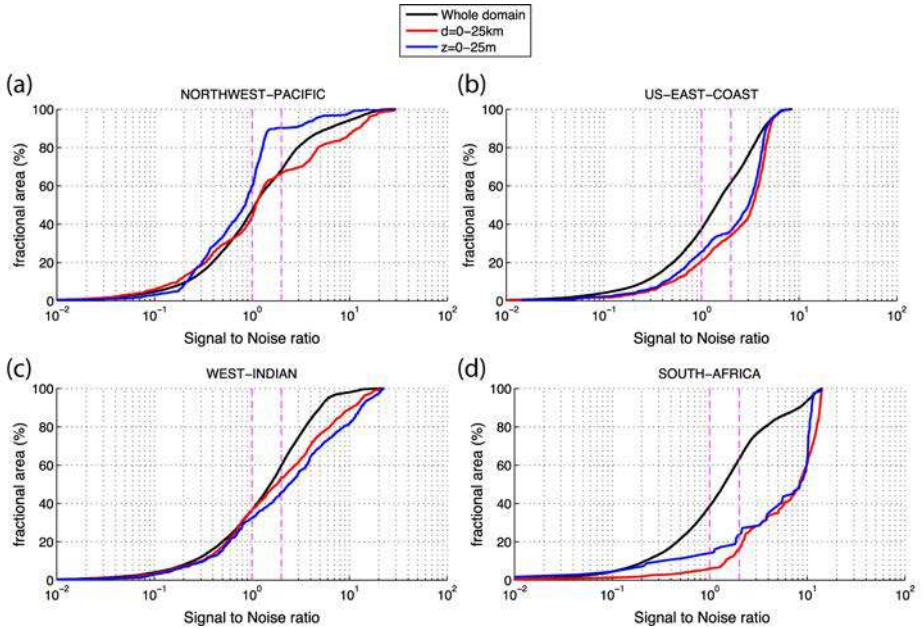


Fig. 5 Same as Fig. 4c for the four domains shown in Fig. 3 (with identically laid out panels)

global scale (Fig. 4c): while SNR values are smaller than 2 over most (62%) of the SA full domain, this proportion sharply decreases (17–23%) near the coasts and in shallow areas, except along the northeastern coasts of South Africa and the southeastern coast of Mozambique where the SNR remains smaller than 2 (and even less locally, see Fig. 3d). As in the global ocean, the decrease of SNR values in the coastal and shallow areas of the SA domain is essentially due to a sixfold decrease of the median (and more than a tenfold decrease of the maximum) of the LFCIV-induced noise, while the median of the signal remains very close to 1 mm/year (not shown). These resemblances suggest that in several parts of the global ocean, approaching the coastal and shallow oceans has comparable impacts on the forced and random parts of sea-level trends as in the SA region.

Figure 5b resembles Fig. 5d: within the whole region shown in Fig. 3b, SNR values are smaller than 2 over 62% of model grid points, and over substantially less (36–38%) grid points in its coastal and shallow parts, with a strong spatial inhomogeneity: coastal sea-level trends can be attributed to the forcing along most of US Atlantic coast (SNR > 2 from around Titusville, FL, to Nova Scotia at least) and along the coasts of the Caribbean islands. In contrast, our results suggest that coastal sea-level trends may be random over most of the Gulf of Mexico coastline (from southwest Florida to the southernmost point of the Gulf), with SNR values remaining even smaller than 0.5 everywhere between Pensacola, FL, to Caillou Bay, LO.

The structure of the forced and random trends is much more homogeneous along the coasts of the northwestern Pacific (NWP) domain, host of the strongly turbulent Kuroshio. Here as well, the SNR remains below 2 within most (about 68%) of its total area. In contrast with the other regions considered, however, this fractional area remains as large when only coastal regions are considered, and even increases (90%) in the shallow parts of the NWP domain. Figure 3a further shows that the sea-level trend SNR

Table 1 Main statistics (last 3 lines) of total, steric, and manometric sea-level trends (last three columns) over the global ocean: whole domain (black), grid points within 25 km of the coasts (red), grid points with depth shallower than 25 m (blue)

GLOBAL OCEAN:			Total sea level trends			Steric sea level trends			Manometric sea level trends		
Whole	Coastal	Shallow									
Median of the Signal Absolute value (Forced sea level trends, mm/yr)			1.0	1.0	1.0	1.0	0.9	0.9	0.1	0.4	1.0
Median of the Noise (Random sea level trends, mm/yr)			0.3	0.1	0.1	0.3	0.045	0.025	0.05	0.09	0.1
Fractional area where $S/R < 2$			38%	17%	20%	37%	5%	1%	56%	30%	14%

remains smaller than 2 (and becomes locally much smaller) almost everywhere along the continental and island coastlines located within the East China Sea, Yellow Sea, and Japan Sea, all the way between the cities of Haikou (South China) and Vladivostok, including most Japanese coastlines (except southern and northeastern Hokkaido). Further analysis in the NWP region (not shown) shows that the median forced sea-level trends now decrease by a factor 4–6 near the coasts and in shallow waters compared to the open ocean, while the imprint of LFCIV on these trends only decreases by a factor of 3, yielding these small SNR values over most of the coasts in this area. The NWP domain is therefore the region of the global ocean where attributing coastal sea-level trends to external drivers is the most questionable.

3.3 Steric and Manometric Contributions to the Coastal Sea-Level Trend Components

The total regional sea-level trends discussed above may be split in two components: steric trends result from the thermal expansion and haline contraction of seawater, and manometric (i.e., non-steric) sea-level trends come from local changes in the mass of seawater at each location. Note that the trends in the melting rate of glaciers and ice sheets are not taken into account in these simulations.

In this section, we investigate the respective imprints of steric and manometric components on the forced and random trends over the global ocean area, and in its shallow (SD), and coastal (CD) parts. Table 1 summarizes for each of these three domains the forced part, the random part, and the SNR of the total, steric and manometric regional sea-level trends. The last three lines in Table 1 are derived from the counterparts of Fig. 4 drawn for the steric and manometric sea-level trends (not shown); colors correspond to the whole global ocean, its coastal and shallow parts.

3.3.1 Steric and Manometric Coastal Sea-Level Trends: Forced Part

The second line in Table 1 concerns the median of the absolute value of the signal (i.e., of the forced trends). In Fig. 4a, this median corresponds to the abscissae where each line reaches the 50% fractional area. As explained in the previous section, the median absolute values of the forced total sea-level trends are basically the same over the open ocean, the coastal and shallow domains (close to 1 mm/year, see line 2, column 2). The next two columns of line 2 further indicate that forced steric trends are also typically close to 1 mm/year in absolute value over these 3 domains, but that forced manometric trends (last column) are 4 and 10 times stronger in the coastal and shallow domains, respectively.

This strong increase of forced manometric trends toward the coast is consistent with several studies using forced ocean circulation models (Griffies and Greatbatch 2012) and coupled climate models (Landerer et al. 2007a, b; Yin et al. 2009, 2010) at coarse resolution. Sea-level projections in the late twenty-first century show an increase of bottom pressure loading along shelves and marginal seas related to the expansion of open ocean water due to the increased concentration of greenhouse gases in the atmosphere. Such a forced increase of ocean heat content in the open ocean may create a steric sea-level gradient next to the continental shelf and push water masses toward the coast at the shelf break. As the deep open ocean can absorb more heat than shallower coastal regions, steric sea-level trends can be greater away from the coastal zone. Therefore, the steric sea-level change yields a dynamic topography gradient near the continental shelf areas, with lower dynamic topography on the shelves than in the open oceans. Dynamic topography gradients may then locally modify ocean currents through dynamical adjustments. Therefore, open ocean water is expected to progressively penetrate on the shelves, increase mass and therefore ocean bottom pressure in the coastal areas, yielding this enhanced forced manometric sea-level trend near the coasts.

3.3.2 Steric and Manometric Coastal Sea-Level Trends: Random Part

The third line in Table 1 concerns the median of the noise (random trends). In Fig. 4b, this median corresponds to the abscissae where each line reaches 50% fractional area. As mentioned in Sect. 3.2.1, the median amplitude of random total sea-level trends is close to 0.3 mm/year over the whole global ocean area, i.e., about 30% of the typical forced signal. Unlike the forced (total and steric) sea-level trends which were similar in the whole, coastal and shallow regions, typical values of their random counterparts drop by 70–99% when only coastal and shallow domains are considered (columns 2 and 3, line 3).

As was noted for its forced counterpart, the manometric random sea-level trend median increases (roughly doubles) from the open ocean to its coastal and shallow parts, and gets similar as the total random trend median (about 0.1 mm/year). This amplification toward the coasts of manometric trends thus concerns both the forced and random components, unlike the steric trends whose medians remain unchanged (forced component) or sharply drop (random component). The dynamical hypotheses presented in Sect. 3.3.1 to explain the coastal amplification of forced manometric trends are likely to hold for their random counterparts.

3.3.3 Steric and Manometric Coastal Sea-Level Trends: Signal-to-Noise Ratio

The reader might have noted that adding the medians of steric and manometric sea-level trends (columns 3 and 4 in lines 2 or 3) does not yield the median of total sea-level trends (column 2). Indeed, the fractional areas corresponding to steric and manometric components are computed independently after sorting their values by increasing order. In other words, the values given in rows 2 and 3 of Table 1 do not take into account the possibility of local compensations between steric and manometric signals. These possible compensations are now taken into account: the last line of the table gives the fraction of the area of the global ocean (full, coastal, and shallow domains) where the *local* signal-to-noise ratios (SNR) of total, steric, and manometric sea-level trends are smaller than 2. This is the percentage of the area where regional trends cannot be unambiguously attributed to external causes (95% confidence), but may be due to the LFCIV.

As mentioned earlier, attributing total sea-level trends to the atmospheric forcing is questionable over 38% of the global ocean area; this fraction decreases to 17–20% in its coastal and shallow parts (line 4, column 2). The changes of the forced and random parts of the steric and manometric signals when approaching the coast (described above separately) combine together when considering them locally, and yield a simpler picture in terms of SNR: the fractional area over which the oceanic LFCIV may affect the (steric, manometric, and total) sea-level trends consistently decrease when switching from the global ocean to its coastal and shallow parts. In the coastal regions located within 25 km of the coasts, the external forcing cannot be certainly held as the main driver of total sea-level trends over 17% of the oceanic area. This area proportion is slightly larger (30%) for manometric sea-level trends, and clearly smaller for steric sea-level trends (5%).

In summary, our results show that sea-level trends in coastal regions are somewhat shielded from the LFCIV, whose relative contribution compared to the forced signal is smaller than in the open ocean. The attribution of coastal sea-level trends to external forcing (atmospheric fluctuations, anthropogenic forcing) is thus valid over most of the globe, but requires care in regions where the SNR approaches 2, and may be invalid where SNR values drop below this level (i.e., within 17–20% of the global ocean coastal area). The model suggests that sea-level trends in such regions may be random since they are substantially impacted by the ocean-driven low-frequency chaotic variability.

4 Conclusions and Discussion

Sea-level trends have a complex distribution along the coasts, where the ongoing global mean sea-level rise can be either enhanced or reduced. The accurate monitoring and understanding of these coastal trends requires detailed analyses of their causes, and of the associated uncertainties. In this paper, we investigated the contributions of two drivers of coastal sea-level trends over the altimetric period (1993–2015): the trends driven by the atmospheric evolution (of natural or anthropic origin), and the trends driven by the oceanic Low-Frequency Chaotic Intrinsic Variability (LFCIV). The latter driver is substantial when mesoscale eddies are (even partly) resolved, and should be considered as a source of uncertainty for attributing coastal sea-level trends to external drivers: the LFCIV indeed induces random fluctuations on sea-level trends and other oceanic fields.

Using the outputs of a large ensemble of $1/4^\circ$ global oceanic hindcasts, we showed that, in certain coastal areas, this “noise” may blur the detection of regional sea-level trends.

Our results do not concern (and do not question the anthropic origin of) the globally averaged 1993–2015 sea-level trend, which was removed from our datasets: they concern the regional contrasts of sea-level trends near the coasts, specifically their external or internal origin. Our main results may be summarized as follows:

- Coastal sea-level trends are not significantly impacted by the ocean-driven multi-decadal LFCIV over most (80–83%) of the global ocean area located less than 25 km away from the coasts. They may be attributed to non-oceanic (atmospheric or anthropic) causes with 95% confidence level.
- However, coastal sea-level trends cannot be unambiguously attributed to atmospheric drivers over the remaining 17–20% of the global ocean coastal area. There, the ocean-driven multi-decadal LFCIV is smaller than in the open ocean, but still induces random sea-level trends that represent more than half of the externally driven counterpart, and may blur the detection of the latter.
- These latter regions are inhomogeneously distributed around the globe and sit near strong eddy-active regions (Fig. 3). They include in particular all island and continental coastlines between 142°E and the Asian coast between 20 and 42°N , most of the Gulf of Mexico coastline, and several parts of the northwestern Indian Ocean coastlines.
- Steric sea-level trends are impacted by LFCIV over only 5% of the global ocean coastal area; manometric sea-level trends are impacted by LFCIV over a larger fraction (30%) of it.

These results suggest that the presently available 23-year altimeter record is not long enough to rigorously assess the externally forced character of sea-level trends along 17–20% of the coastlines. It is nevertheless likely that a longer altimetric record will progressively increase the percentage of coastal areas where the LFCIV does not perturb the attribution of sea-level changes. In this context, an interesting perspective of this study would be to assess the contribution of atmospherically forced and internally generated sea-level trends in coastal regions where (longer) tide gauge records are available.

The members of this ensemble simulation represent the observed distribution of regional sea-level trends with a very good degree of accuracy in the open ocean (as quantified in Llovel et al. 2018), except in a few areas such as the western Subpolar Gyre of the North Atlantic. As for any model-based study however, our results should be considered with caution. The fidelity of $1/4^\circ$ simulations may decrease from the open ocean toward the coasts: certain coastal processes are either absent from our model (e.g., tides, surface gravity waves, etc.), or may be marginally resolved (mesoscale turbulence, edge waves, coastal wind drop-off, certain upwellings, etc.) since depth, hence the internal Rossby radii and the model effective resolution, generally decrease when approaching the coasts. Future investigations of forced and random coastal sea-level trends could utilize for instance higher resolution ensembles of regional coastal simulations (with adequate lateral forcing), and ideally ensembles gathering different types of models. The present study may in any case be seen as a proof of concept: it illustrates at least the potential of ensemble-based modeling strategies for disentangling internal and external sources of oceanic fluctuations over a wide range of scales.

As noted in Sect. 1.2, the ocean-driven LFCIV, and therefore random sea-level trends, are largely underestimated in laminar ocean simulations forced by the atmosphere, and presumably also in ocean–atmosphere coupled simulations where the oceanic mesoscale

is absent. In other words, the LFCIV is an oceanic driver of coastal sea-level changes in the turbulent regime, which may compete with the external drivers examined in Woodworth et al. (2019) and with the ocean–atmosphere coupled modes presented by Han et al. (2019). More importantly, the random character of LFCIV suggests that it actually constitutes a source of uncertainty for the detection and attribution of coastal sea-level trends, in addition to those simulated by climate models (Carson et al. 2019), and that these uncertainties should also be taken into account for coastal sea-level projections (see Jevrejeva et al. 2019).

Fasullo and Nerem (2018) and Hamlington et al. (2019) used ocean–atmosphere coupled ensemble simulations (with a non-eddy ocean component) to extract the “internal” and “forced” sea-level trends. In their context however, (1) “internal” refers to the variability (e.g., ENSO, PDO, etc.) and trends that emerge from the air–sea coupling and in the turbulent atmosphere, whose phase are essentially random and differ among ensemble members; (2) “forced” refers to the response of the coupled system to the sole anthropogenic forcing (greenhouse gases concentration increase in particular).

In our study, we have used an ocean-only ensemble simulation (with an eddy ocean model) driven by a prescribed atmospheric variability. As explained in Sérazin et al. (2017, their introduction) and in Penduff et al. (2018), this prescription of the atmospheric variability is mandatory to split the oceanic variability into its atmospherically forced component, and its intrinsic/chaotic variability that spontaneously arises in the turbulent ocean. In other words, what we called the “forced” ocean variability and trends are those driven by the atmospheric forcing (including the anthropogenic trends it contains), and what we called the LFCIV and the random trends emerge in the ocean from nonlinear processes without coupling to the atmosphere. It is important to recall, as mentioned in Sect. 1.2, that this oceanic LFCIV is very small in non-eddy ocean models (Penduff et al. 2011; Grégorio et al. 2015): Fasullo and Nerem (2018) and Hamlington et al. (2019)’s coupled simulations performed with a non-eddy ocean are thus certainly underestimating this chaotic variability that our eddy ocean model generates. In other words, the processes and signals that we have disentangled are distinct from those considered in the latter two studies.

Characterizing the imprints of LFCIV on, e.g., sea-level trends in a global eddy 50-member ensemble simulation coupled to the atmosphere would not only require huge computational resources; it would also require simulation and analysis strategies allowing to separate intrinsic and forced signals within two fluids in complex interaction, and such strategies are not clear yet. An intermediate step could consist of forcing atmospheric model ensembles with sea-surface temperature (or upper ocean heat content) fields simulated in several OCCIPUT members. This would help to answer important but open questions about the atmospheric response to random trends of the upper ocean heat content (Sérazin et al. 2017), which contribute to the steric sea-level trends discussed here. These ambitious modeling and physical objectives are left for the future.

Acknowledgements This work is a contribution to the OCCIPUT and PIRATE projects. PIRATE (<https://sealevel.jpl.nasa.gov/science/ostscienceteam/scientistlinks/scientificinvestigations2017/penduff/>) is funded by CNES through the Ocean Surface Topography Science Team (OST-ST). OCCIPUT (<https://meom-group.github.io/projects/occiput/>) was funded by ANR through contract ANR-13-BS06-0007-01. This work was also supported by the French national program LEFE/INSU and has received funding from the European Union Horizon 2020 research and innovation program under grant agreement No 633211. It is also part of the Copernicus Marine Environment Monitoring Service (CMEMS) GLO-HR project; CMEMS is implemented by Mercator Ocean International in the framework of a delegation agreement with the European Union. We acknowledge that the results of this research have been achieved using the PRACE Research Infrastructure resource CURIE based in France at TGCC. William Llovel was supported by C3S program, “Louis Gentil–Jacques Bourcart” fellowship from the French Académie des Sciences and by the OVALIE

project from ESA Living Planet Fellowship fundings. The CCI product is freely available at <http://www.esa-sealevel-cci.org/>. The model dataset used for this study is freely available on <http://zenodo.org> (<http://doi.org/10.5281/zenodo.1487983>). We would like to thank two anonymous reviewers for their constructive comments and helpful suggestions.

References

- Ablain M, Legeais JF, Prandi P, Marcos M, Fenoglio-Marc L, Dieng HB, Benveniste J, Cazenave A (2017) Satellite altimetry-based sea level at global and regional scales. *Surv Geophys* 38:7–31. <https://doi.org/10.1007/s10712-016-9389-8>
- Bessières L, Leroux S, Brankart J-M, Molines J-M, Moine M-P, Bouttier P-A, Penduff T, Terray L, Barnier B, Sérazin G (2017) Development of a probabilistic ocean modelling system based on NEMO 3.5: application at eddying resolution. *Geosci Model Dev* 10:1091–1106. <https://doi.org/10.5194/gmd-10-1091-2017>
- Brankart J-M (2013) Impact of uncertainties in the horizontal density gradient upon low resolution global ocean modelling. *Ocean Model* 66:64–76
- Carson M, Lyu K, Richter K, Becker M, Domingues CM, Han W, Zanna L (2019) Climate model uncertainty and trend detection in regional sea level projections: a review. *Surv Geophys*. <https://doi.org/10.1007/s10712-019-09559-3>
- Church JA, White NJ, Konikow LF, Domingues CM, Cogley JG, Rignot E, Gregory JM, van den Broeke MR, Monaghan AJ, Velicogna I (2011) Revisiting the Earth's sea-level and energy budgets from 1961 to 2008. *Geophys Res Lett* 38:L18601. <https://doi.org/10.1029/2011GL048794>
- Church JA, Clark PU, Cazenave A, Gregory JM, Jevrejeva S, Levermann A, Merrifield MA, Milne GA, Nerem RS, Nunn PD, Payne AJ, Pfeffer WT, Stammer D, Unnikrishnan AS (2013) Sea level change. In: Stocker TF, Qin D, Plattner G-K, Tignor M, Allen SK, Boschung J, Nauels A, Xia Y, Bex V, Midgley PM (eds) *Climate change 2013: the physical science basis. Contribution of working group I to the fifth assessment report of the intergovernmental panel on climate change*. Cambridge University Press, Cambridge and New York
- Dussin R, Barnier B (2013) The making of DFS5.1. Drakkar project report, Grenoble, France
- Fasullo JT, Nerem RS (2018) Altimeter-era emergence of the patterns of forced sea-level rise in climate models and implications for the future. *Proc Nat Acad Sci* 115(51):12944–12949. <https://doi.org/10.1073/pnas.1813233115>
- Greatbatch RJ (1994) A note on the representation of steric sea level in models that conserve volume rather than mass. *J Geophys Res* 99(C6):12767–12771
- Grégorio S, Penduff T, Sérazin G, Molines J-M, Barnier B, Hirschi J (2015) Intrinsic variability of the Atlantic meridional overturning circulation at interannual-to-multidecadal time scales. *J Phys Oceanogr* 45(7):1929–1946. <https://doi.org/10.1175/JPO-D-14-0163.1>
- Gregory JM, Griffies SM, Hughes CW et al (2019) Concepts and terminology for sea level: mean, variability and change, both local and global. *Surv Geophys*. <https://doi.org/10.1007/s10712-019-09525-z>
- Griffies SM, Greatbatch RJ (2012) Physical processes that impact the evolution of global mean sea level in ocean climate models. *Ocean Model* 51:37–72. <https://doi.org/10.1016/j.ocemod.2012.04.003>
- Griffies SM, Yin J, Durack PJ, Goddard P, Bates SC, Behrens E, Bentsen M, Bi D, Biastoch A, Böning C, Bozec A, Chassignet E, Danabasoglu G, Danilov S, Domingues CM, Drange H, Farneti R, Fernandez E, Greatbatch RJ, Holland DM, Ilicak M, Large WG, Lorbacher K, Lu J, Marsland SJ, Mishra A, Nurser AJG, Salas-Méllia D, Palter JB, Samuels BL, Schröter J, Schwarzkopf FU, Sidorenko D, Treguier A-M, Tseng YH, Tsujino H, Uotila P, Valcke S, Voldoire A, Wang Q, Winton M, Zhang X (2014) An assessment of global and regional sea level for years 1993–2007 in a suite of interannual CORE-II simulations. *Ocean Model* 78:35–89. <https://doi.org/10.1016/j.ocemod.2014.03.004>
- Hallberg R (2013) Using a resolution function to regulate parameterizations of oceanic mesoscale eddy effects. *Ocean Model* 72:92–103. <https://doi.org/10.1016/j.ocemod.2013.08.007>
- Hamlington BD, Fasullo JT, Nerem RS, Kim KY, Landerer FW (2019) Uncovering the pattern of forced sea level rise in the satellite altimeter record. *Geophys Res Lett* 46(9):4844–4853. <https://doi.org/10.1029/2018GL081386>
- Han W, Stammer D, Thompson P, Ezer T, Palanisamy H, Zhang X, Domingues CM, Zhang L, Yuan D (2019) Impacts of basin-scale climate modes on coastal sea level: a review. *Surv Geophys*. <https://doi.org/10.1007/s10712-019-09562-8>

- Hirschi J, Baehr J, Marotzke J, Stark J, Cunningham S, Beismann J-O (2003) A monitoring design for the Atlantic meridional overturning circulation. *Geophys Res Lett* 30:1413. <https://doi.org/10.1029/2002GL016776>
- Huck T, Arzel O, Sévellec F (2015) Multidecadal variability of the overturning circulation in presence of eddy turbulence. *J Phys Oceanogr* 45(1):157–173. <https://doi.org/10.1175/jpo-d-14-0114.1>
- Jevrejeva S, Frederikse T, Kopp RE, Le Cozannet G, Jackson LP, van de Wal RSW (2019) Probabilistic sea level projections at the coast by 2100. *Surv Geophys*. <https://doi.org/10.1007/s10712-019-09550-y>
- Landerer F, Jungclaus J, Marotzke J (2007a) Ocean bottom pressure changes lead to a decreasing length-of-day in a warming climate. *Geophys Res Lett* 34:L06307. <https://doi.org/10.1029/2006GL029106>
- Landerer F, Jungclaus J, Marotzke J (2007b) Regional dynamic and steric sea level change in response to the IPCC-A1B scenario. *J Phys Oceanogr* 37:296–312
- Legéais J-F, Ablain M, Zawadzki L, Zuo H, Johannessen JA, Scharffenberg MG, Fenoglio-Marc L, Fernandes MJ, Andersen OB, Rudenko S, Cipollini P, Quartly GD, Passaro M, Cazenave A, Benveniste J (2018) An improved and homogeneous altimeter sea level record from the ESA Climate Change Initiative. *Earth Syst Sci Data* 10:281–301. <https://doi.org/10.5194/essd-10-281-2018>
- Leroux S, Penduff T, Bessières L, Molines J, Brankart J, Sérazin G, Barnier B, Terray L (2018) Intrinsic and atmospherically forced variability of the AMOC: insights from a large-ensemble ocean hindcast. *J Clim* 31:1183–1203. <https://doi.org/10.1175/JCLI-D-17-0168.1>
- Llovel W, Lee T (2015) Importance and origin of halosteric contribution to sea level change in the southeast Indian Ocean during 2005–2013. *Geophys Res Lett* 42:1148–1157
- Llovel W, Penduff T, Meyssignac B, Molines J-M, Terray L, Bessières L, Barnier B (2018) Contributions of atmospheric forcing and chaotic ocean variability to regional sea level trends over 1993–2015. *Geophys Res Lett*. <https://doi.org/10.1029/2018GL080838>
- Marcos M, Wöppelmann G, Matthews A, Ponte RM, Birol F, Arduin F, Coco G, Santamaria-Gomez A, Ballu V, Testut L, Chambers D, Stop JE (2019) Coastal sea level and related fields from existing observing systems. *Surv Geophys*. <https://doi.org/10.1007/s10712-019-09513-3>
- Nerem RS, Beckley BD, Fasullo JT, Hamlington BD, Masters D, Mitchum GT (2018) Climate-change-driven accelerated sea-level rise detected in the altimeter era. *Proc Natl Acad Sci USA* 115(9):2022–2025. <https://doi.org/10.1073/pnas.1717312115>
- O’Kane TJ, Matear RJ, Chamberlain MA, Risbey JS, Sloyan BM, Horenko I (2013) Decadal variability in an OGCM Southern Ocean: intrinsic modes, forced modes and metastable states. *Ocean Model* 69:1–21. <https://doi.org/10.1016/j.ocemod.2013.04.009>
- Penduff T, Juza M, Barnier B, Zika J, Dewar WK, Treguier A-M, Molines J-M, Audiffren N (2011) Sea-level expression of intrinsic and forced ocean variabilities at interannual time scales. *J Clim* 24:5652–5670. <https://doi.org/10.1175/JCLI-D-11-00077.1>
- Penduff T, Barnier B, Terray L, Bessières L, Sérazin G, Grégorio S, Brankart J-M, Moine M-P, Molines J-M, Brasseur P (2014) Ensembles of eddying ocean simulations for climate. *CLIVAR Exchanges, Special Issue on High Resolution Ocean Climate Modelling*, 65, vol 19, no 2, July 2014
- Penduff T, Sérazin G, Leroux S, Close S, Molines JM, Barnier B, Bessières L, Terray L, Maze G (2018) Chaotic variability of ocean: heat content climate-relevant features and observational implications. *Oceanography* 31(2):63–71. <https://doi.org/10.5670/oceanog.2018.210>
- Rhein M, Rintoul SR, Aoki S, Campos E, Chambers D, Feely RA, Gulev S, Johnson GC, Josey SA, Kostianoy A et al (2013) Observations: ocean. Chapter 3 in climate change 2013: the physical science basis. In: Stocker TF, Qin D, Plattner G-K, Tignor M, Allen SK, Boschung J, Nauels A, Xia Y, Bex V, Midgley PM (eds) *Contribution of working group I to the fifth assessment report of the intergovernmental panel on climate change*. Cambridge University Press, Cambridge
- Sérazin G, Penduff T, Grégorio S, Barnier B, Molines J-M, Terray L (2015) Intrinsic variability of sea-level from global 1/12° ocean simulations: spatio-temporal scales. *J Clim* 28:4279–4292. <https://doi.org/10.1175/JCLI-D-14-00554>
- Sérazin G, Meyssignac B, Penduff T, Terray L, Barnier B, Molines J-M (2016) Quantifying uncertainties on regional sea-level rise induced by multi-decadal oceanic intrinsic variability. *Geophys Res Lett*. <https://doi.org/10.1002/2016GL069273>
- Sérazin G, Jaymond A, Leroux S, Penduff T, Bessières L, Llovel W, Barnier B, Molines J-M, Terray L (2017) A global probabilistic study of the ocean heat content low-frequency variability: atmospheric forcing versus oceanic chaos. *Geophys Res Lett* 44:5580–5589. <https://doi.org/10.1002/2017GL073026>
- Sérazin G, Penduff T, Barnier B, Molines J, Arbic BK, Müller M, Terray L (2018) Inverse cascades of kinetic energy as a source of intrinsic variability: a global OGCM study. *J Phys Oceanogr* 48:1385–1408. <https://doi.org/10.1175/JPO-D-17-0136.1>

- WCRP Global Sea Level Budget Group (2018) Global sea-level budget 1993–present. *Earth Syst Sci Data* 10:1551–1590. <https://doi.org/10.5194/essd-10-1551-2018>
- Woodworth PL, Melet A, Marcos M, Ray RD, Wöppelmann G, Sasaki YN, Cirano M, Hibbert A, Huthnance JM, Monserrat S, Merrifield MA (2019) Forcing factors affecting sea level changes at the coast. *Surv Geophys*. <https://doi.org/10.1007/s10712-019-09531-1>
- Yin J, Schlesinger M, Stouffer R (2009) Model projections of rapid sea-level rise on the northeast coast of the United States. *Nat Geosci* 2:262–266
- Yin J, Griffies SM, Stouffer R (2010) Spatial variability of sea-level rise in 21st century projections. *J Clim* 23:4585–4607
- Zanna L, Brankart JM, Huber M, Leroux S, Penduff T, Williams PD (2018) Uncertainty and scale interactions in ocean ensembles: from seasonal forecasts to multi-decadal climate predictions. *Q J R Meteorol Soc*. <https://doi.org/10.1002/qj.3397>